# Imaging salt bodies using explicit migration operators offshore Norway

Børge Arntsen[1], Constantin Gerea[2], and Tage Røsten[3]

## ABSTRACT

We have tested the performance of 3D shot-profile depth migration using explicit migration operators on a real 3D marine data set. The data were acquired offshore Norway in an area with a complex subsurface containing large salt bodies. We compared shot-profile migration using explicit migration operators with conventional Kirchhoff migration, split-step Fourier migration, and common-azimuth by generalized screen propagator (GSP) migration in terms of quality and computational cost. Image quality produced by the explicit migration operator approach is slightly better than with split-step Fourier migration and clearly better than in common-azimuth by GSP and Kirchhoff migrations. The main differences are fewer artifacts and better-suppressed noise within the salt bodies. Kirchhoff migration shows considerable artifacts (migration smiles) within and close to the salt bodies, which are not present in images produced by the other three wave-equation methods. Expressions for computational cost were developed for all four migration algorithms in terms of frequency content and acquisition parameters. For comparable frequency content, migration cost using explicit operators is four times the cost of the split-step Fourier method, up to 260 times the cost of common-azimuth by GSP migration, and 25 times the cost of Kirchhoff migration. Our results show that in terms of image quality, shot-profile migration using explicit migration operators is well suited for imaging in areas with complex geology and significant velocity changes. However, computational cost of the method is high and makes it less attractive in terms of efficiency.

## INTRODUCTION

Holberg (1988) introduces shot-profile migration with explicit operators to allow optimum one-way wave propagation and imaging in areas with large lateral velocity changes. The method is extended to three dimensions by Blacquière et al. (1989) and essentially involves recursive use of a 2D complex convolutional operator across the migration aperture in the space-frequency domain. Because of the convolution, the algorithm is computationally expensive but has the advantage of being able to handle very complex velocity models. Hale (1991a; 1991b) introduces McClellan transforms to exploit the inherent symmetry of the 3D migration operator and reduce computational cost substantially. Using similar approaches, Sollid and Arntsen (1994) and Soubaras (1992) also designed effective 3D migration schemes.

Mittet (2007) proposes a fast and flexible convolutional 3D migration operator that also makes full use of the rotational symmetry of 3D migration operators. We apply a version of Mittet's (2007) proposed migration operator to a real data set of realistic industrial size and evaluate its performance implemented as shot-profile migration by direct comparison with conventional Kirchhoff migration, split-step Fourier shot-profile migration (Stoffa et al. 1990), and common-azimuth by generalized-screen propagator (GSP) migration (Biondi and Palacharla, 1996; De Hoop et al., 2000; Le Rousseau and De Hoop, 2001; Le Rousseau et al., 2003). The last three algorithms are all less demanding in terms of computer resources than the explicit-operator method and are often preferred because of economic reasons. By direct comparison of the explicit-migration-operator method with three other widely used algorithms, we can evaluate trade-offs between quality and cost in a realistic setting.

We use a marine data set and velocity model from offshore Norway. This data set features large salt bodies surrounded by sediments. The most challenging aspect — lateral velocity changes associated with the salt — should provide a good opportunity for migration algorithm testing. Shot-profile migration using explicit migration operators gives slightly better quality images than the split-step Fourier method and better than common-azimuth by GSP, but it is also the most expensive in terms of computer resources. Images produced by conventional Kirchhoff migration show substantial migration smiles not present in images produced by migration with explic-

it-migration operators, the split-step Fourier algorithm, or common-azimuth by GSP migration.

Next we review 3D shot-profile migration with explicit operators, split-step Fourier, common-azimuth by GSP, and Kirchhoff migration, before we describe the data set and velocity model. Later we compare results of shot-profile migration using explicit migration operators with other migration algorithms.

## 3D MIGRATION ALGORITHMS

Shot-profile migration algorithms (Claerbout, 1971) can be expressed as wavefield extrapolation of recorded data and a source wavefield, followed by an imaging condition. The wavefield-extrapolation step can be derived from the Kirchhoff integral

$$p(\mathrm{x}, \omega) = -2 \int_S d\mathbf{S} \cdot \nabla \, g^*(\mathrm{x}, \mathrm{x}_s, \omega) q(\mathrm{x}_s, \omega), \qquad (1)$$

where x and $\omega$ denote position and (angular) frequency, respectively, and $p(\mathrm{x}, \omega)$ is the extrapolated wavefield at depth. The integral extends over recording surface $\mathbf{S}$, and $q(\mathrm{x}_s, \omega)$ is the recorded data, where $\mathrm{x}_s$ denotes a position on the recording surface $\mathbf{S}$. The complex conjugate of Green's function is denoted as $g^*(\mathrm{x}, \mathrm{x}_s, \omega)$. The right side of equation 1 is approximated in practice with a recursive expression in depth,

$$p(x, y, z + \Delta z, \omega) = \sum_{i,j = -l}^{l} h(i\Delta x, j\Delta y, \Delta z; k) p$$
$$\times (x + i\Delta x, y + j\Delta x, z; \omega), \quad (2)$$

where $k = \omega/c(x,y,z)$, and $c$ equals wave velocity. Wavefield extrapolation operator $h$ (Mittet, 2007), can be seen as a band-limited numerically optimized approximation to the derivative of Green's function $-2\nabla g(x, x_s', \omega)$. Length of the wavefield extrapolator is denoted by $l$. Equation 2 describes extrapolation of the pressure $p(x, y, z; \omega)$ from depth level $z$ to depth level $z + \Delta z$, where $\Delta z$ is small compared to the seismic wavelength. By starting extrapolation at the surface where pressure is equal to the recorded data, $p(x, y, z$
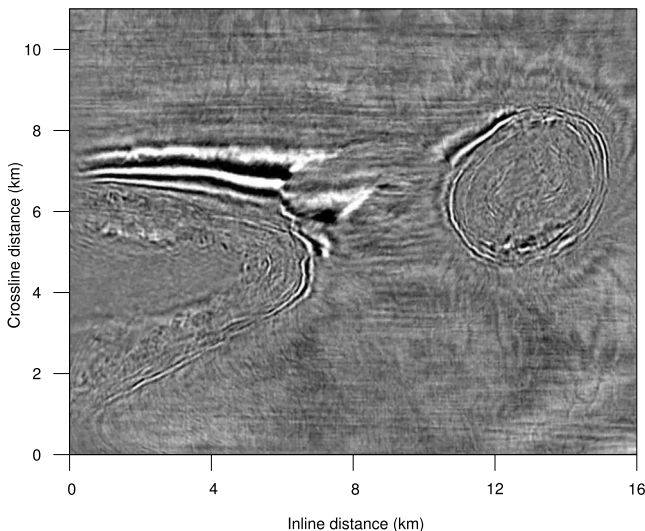


Figure 1. Depth slice at 1000 m, created using Kirchhoff migration, shows two salt dome structures covered by the salt data set.

$= 0; \omega) = q(x, y; \omega)$, equation 2 can be used to estimate the pressure at any depth by repeated application.

Source wavefield $s(\mathrm{x}_s, \omega)$ is known at the surface and extrapolated at depth using equations 1 and 2, but using the Green's function itself instead of its conjugate. An image $r$ (Claerbout, 1971) is obtained by crosscorrelation of the source wavefield and the extrapolated data:

$$r(\mathrm{x}) = \sum_{\omega} p(\mathrm{x}; \omega) s^*(\mathrm{x}; \omega). \qquad (3)$$

Shot-profile split-step Fourier migration (Stoffa et al., 1990) is implemented in a similar manner for migration with explicit operators, with one essential difference: the wavefield extrapolator is given by

$$h_s(x, y, \Delta z, \omega) = f(x, y, \Delta z, \omega)$$
$$\times \exp\{i\omega\Delta z[c^{-1}(x, y, z) - c_0^{-1}]\}. \quad (4)$$

Here $f(x, y, \Delta z, \omega)$ is the Fourier-transform of the phase-shift operator $\exp(i\Delta z\sqrt{\omega^2/c_0^2 - k_x^2 - k_y^2})$, where $c_0$ is an average velocity, and $k_x, k_y$ denote horizontal wavenumbers. Equation 4 is an approximation strictly valid only for small horizontal wavenumbers. The GSP algorithm is a generalization of the split-step Fourier method to improve accuracy for large horizontal wavenumbers and for large dip angles. Biondi and Parlacharla (1996) introduce the common-azimuth migration algorithm, exploiting the fact that most seismic surveys use receiver arrays with limited crossline extension to reduce computational cost significantly. Biondi and Parlacharla's method (1996), known as common-azimuth migration, can be combined with the GSP algorithm to yield the common-azimuth by GSP migration algorithm.

Kirchhoff migration is based on equation 1, but Green's function is approximated with a ray-theoretical expression strictly valid only for very high frequencies. The algorithm is implemented in the time domain, and is reduced in practice to a weighted summation of the input data over traveltime curves.

## THE SALT DATA SET

Our data set from offshore Norway covers a small circular salt-dome structure and parts of a larger salt structure, as shown in Figure 1. Figure 2 is a location map for seismic sections referenced below. Figure 3 shows inline and crossline vertical cross sections of the velocity model, covering the largest salt structure. The most prominent feature of the velocity model is the salt structure and the large velocities associated with it, close to 5000 m/s. Sediments in the area have experienced considerable uplift and erosion, with the result that velocities in the sediments are quite large even at depths close to the seafloor.

Superimposed on the velocity model in Figure 3 are raypaths for a single shotpoint. The structure of the velocity field is such that some raypaths cross, creating multiple raypaths (multipathing) from a source point to a subsurface location. In addition, note the large separation of rays within the salt body, indicating large geometric spreading. This is seen more clearly in Figure 4, which displays the magnitude of the downgoing source field. Downgoing wavefield amplitude is attenuated significantly inside the salt body, and to a certain extent, outside the salt body. The migration velocity field has a strong lateral gradient immediately outside the salt body. This will cause significant differential geometric spreading.

The data underwent standard processing before migration, including editing, designature to achieve zero-phase, and tau-$p$ deconvolution. Because of the large sedimentary velocities near the surface, water-bottom multiples are strong and were attenuated with an extra pass of a Radon-demultiple method. The velocity model in Figure 3 was constructed using a tomographic technique combined with 3D Kirchhoff prestack depth migration. We employed a single-arriv-

al Kirchhoff migration algorithm, using wavefront-construction ray tracing (Vinje et al., 1993) for traveltime computations.

## MIGRATION WITH EXPLICIT OPERATORS VERSUS KIRCHHOFF, FOURIER SPLIT-STEP, AND COMMON-AZIMUTH BY GSP ALGORITHMS

Our data set was first migrated using Kirchhoff migration and common-azimuth by GSP migration. We sorted the same data set used for Kirchhoff and common-azimuth by GSP migrations into shot gathers, as input for 3D shot-profile migrations using explicit migration operators and the split-step Fourier method. We did no additional preprocessing. Because of the large cost of shot-profile migration, we limited the maximum migrated frequency to 35 Hz, but attempted no decimation of shots. Maximum input frequency for Kirchhoff migration was 55 Hz, although the maximum input frequency for common-azimuth by GSP migration was 45 Hz.

Figures 5 and 6 display vertical cross sections for crossline 13700 and inline 7240, respectively. These sections cover the smaller structure visible to the right in Figure 1. Kirchhoff results in Figures 5 and 6 show strong migration smiles close to the salt dome, which are not visible in the shot-profile migration results. The maximum frequency input for Kirchhoff migration is much larger than for the shot-profile migrations, resulting in images with high resolution, particular for shallow sediments. From Figures 5 and 6, we can see that steep parts of the salt-body flanks are better imaged by Kirchhoff migration. The Kirchhoff migration aperture was set to a circle with a radi-
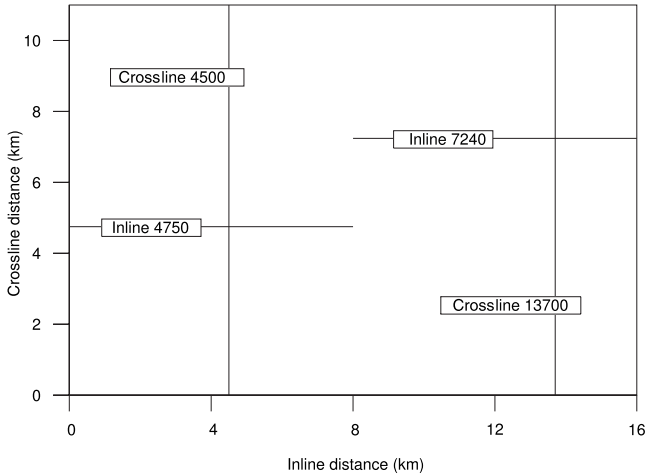


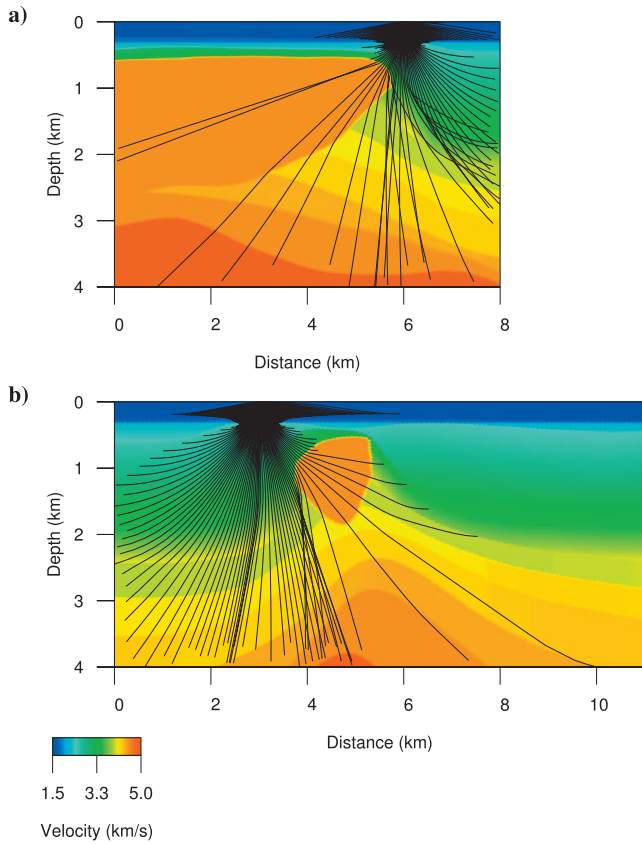Figure 2. Location of the seismic lines.



Figure 3. Velocity model along (a) inline 4750, and (b) crossline 4500. Raypaths from a single source have been overlaid. Note the multipathing problem with crossing rays.
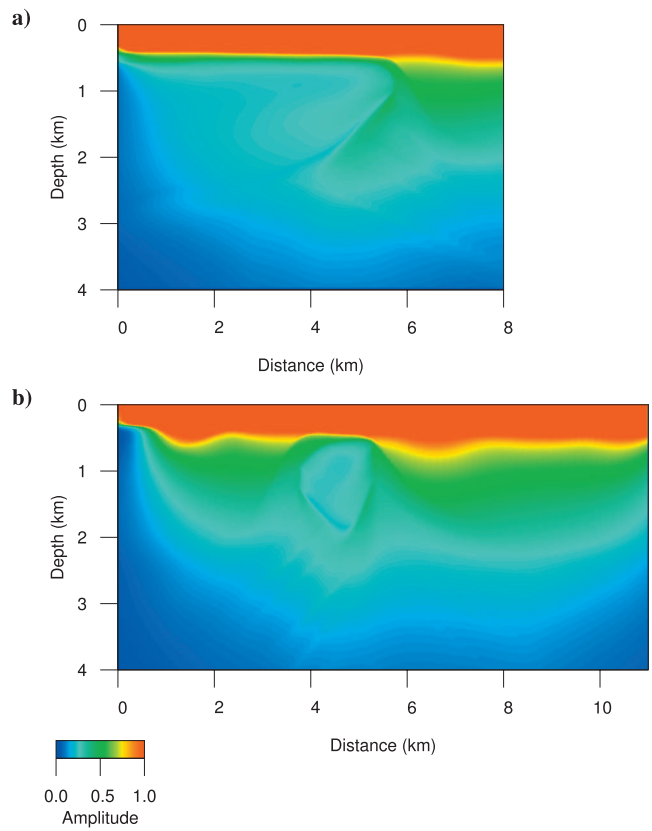


Figure 4. Source illumination map for (a) inline 4750, and (b) crossline 4500. Illumination is poor inside the salt body because of high velocity and large geometric spreading.

us of 4.5 km, and the corresponding aperture for shot-profile migrations was set to a square area with each side equal to 6 km with the source in the center. The smaller aperture might explain why steep-dipping flanks are not imaged properly by shot-profile migrations.

Figure 7 shows depth slices at 2150 meters covering the smallest salt structure on the right side of Figure 1.

Figure 8 depicts the output from shot-profile migration using explicit migration operators extracted along crossline 4500, together with outputs from split-step Fourier shot-profile, common-azimuth by GSP, and Kirchhoff migration. Figure 2 shows the location of the crossline. The Kirchhoff result shows strong migration smiles, which are not visible on the other migration results. The common-azimuth by the GSP migration algorithm produces an image structurally equivalent to images from both shot-profile migration algorithms, but with a slightly higher noise level in areas close to the salt body. However, steep parts of the salt body flanks are better imaged than in shot-profile migrations. This is also true for the Kirchhoff algorithm. Again, a probable cause of this is the limited aperture of shot-profile migrations. The maximum frequency content of common-azimuth by GSP migration is 45 Hz, giving increased reflector resolution compared to shot-profile migrations.

Figure 9 illustrates depth slices at 2100 m, which cover the largest salt structure (seen on the left of Figure 1). The depth slice resulting from Kirchhoff migration has a high noise level, although shot-profile migration depth slices have a comparatively lower level of noise. The maximum frequency used in shot-profile migrations is lower than the maximum frequency used in common-azimuth by GSP and Kirchhoff migration. To allow for a better comparison, we migrated
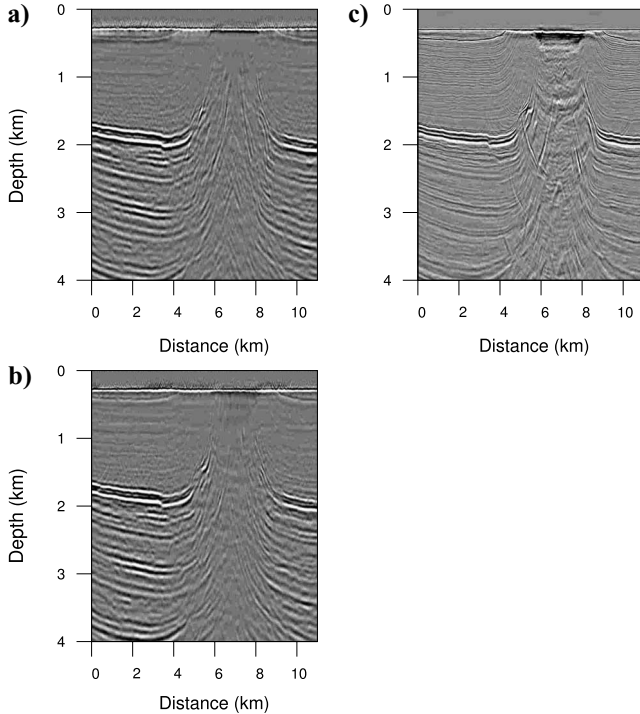


Figure 5. Three–dimensional prestack migration for crossline 13700 using (a) shot-profile migration with explicit migration operators, (b) split-step Fourier shot-profile migration, and (c) Kirchhoff migration. Kirchhoff migration shows significant smiles below approximately 2 km of depth, but images the steep parts of salt flanks better than shot-profile migrations.
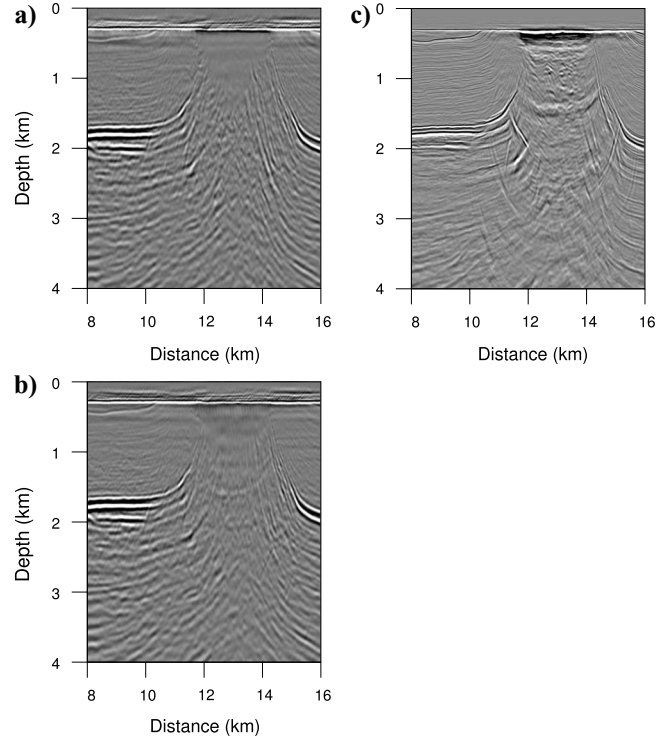


Figure 6. Three–dimensional prestack migration for inline 7240 using (a) shot-profile migration with explicit migration operators, (b) split-step Fourier shot-profile migration, and (c) Kirchhoff migration. Kirchhoff migration shows significant smiles below approximately 2 km of depth, but images the steep parts of the salt flanks better than shot-profile migrations.
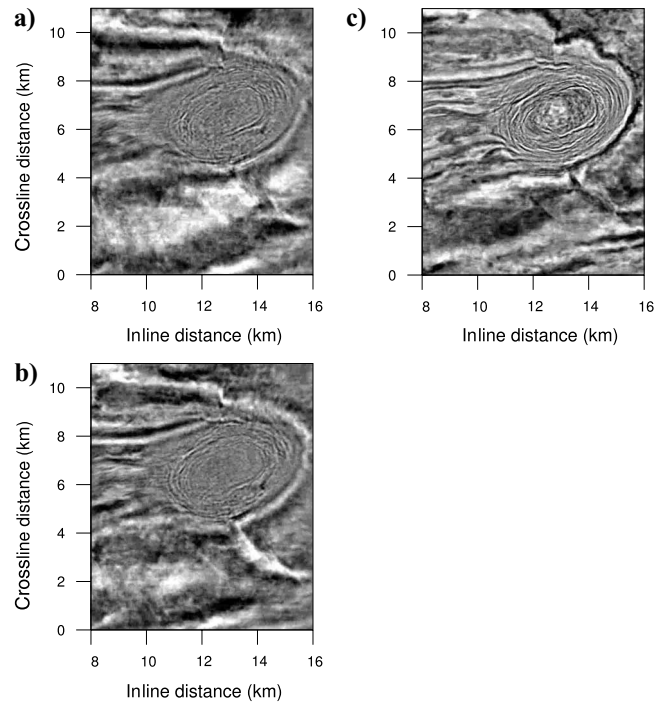


Figure 7. Depth slice at 2150 m, covering the structure shown in the right part of Figure 1 computed with (a) 3D shot-profile migration using explicit operators, (b) split-step Fourier shot-profile migration, and (c) Kirchhoff migration.

half the data set with shot-profile migration using explicit operators with a maximum frequency of 47 Hz. Figure 10 illustrates the result compared with common-azimuth by GSP and Kirchhoff migration. Comparing Figure 8a and Figure 10a, noise and artifacts within the salt body are reduced slightly when the maximum frequency is increased from 35 Hz to 47 Hz. However, smiles in the shallow part of the section (to the left of the salt body) are more apparent in the high frequency image. In addition, some of the deepest reflectors appear less visible on the section with maximum frequency of 47 Hz.

## DISCUSSION

Kirchhoff migration results in Figures 5, 6, and 8 show large migration smiles, which are not present in corresponding sections produced with any of the wave-equation algorithms. A possible explanation is suggested by considering the source illumination map in Figure 4. The source wavefield inside (and close to) the salt bodies is attenuated because of the large geometric spreading caused by high salt velocity. Because the image created by the wave-equation shot-profile migration algorithms involves the product of the source wavefield with the upgoing wavefield (see equation 2), parts of the image inside salt bodies will be attenuated relative to portions of the image outside salt bodies. No significant reflectors exist inside the salt bodies, but residual multiples will appear as apparent reflectors in these areas. In the case of Kirchhoff migration, similar attenuation of the source wavefield does not occur, even if proper amplitude weighting is included (Albertin et al., 2004). This amplitude behavior will contribute in practice to the migration smiles observed.
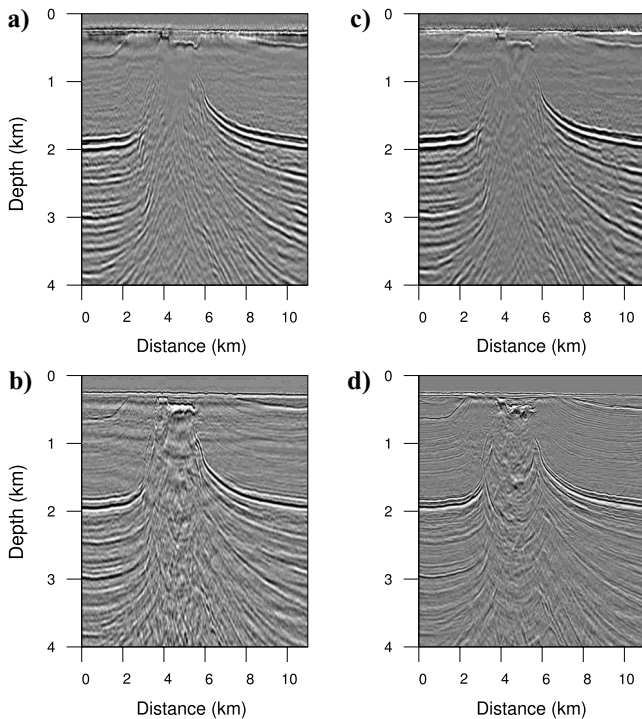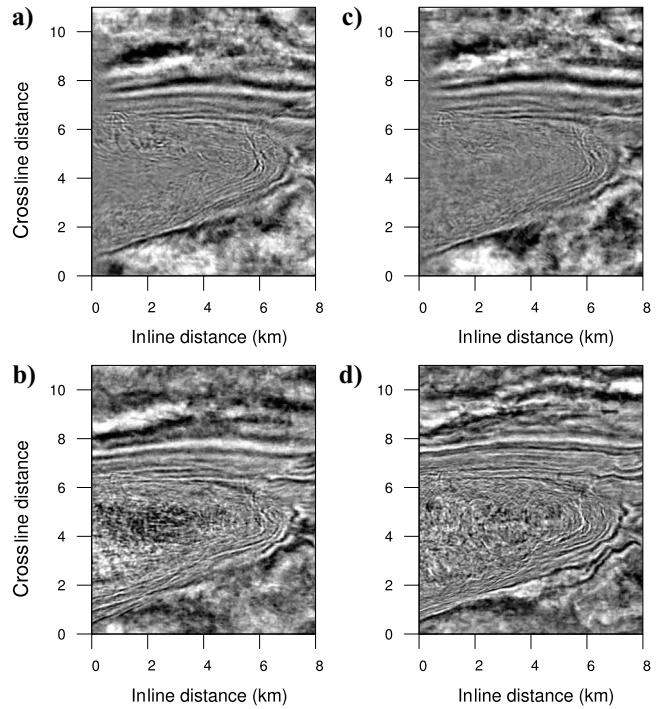
Figure 9. Depth slice at 2100 m, covering the structure shown in the left part of Figure 1 computed with (a) 3D shot-profile migration using explicit operators, (b) common-azimuth by GSP migration, (c) split-step Fourier shot-profile migration, and (d) Kirchhoff migration.

Figure 8. Three–dimensional prestack migration for crossline 4500 using (a) shot-profile migration with explicit migration operators, (b) common-azimuth by GSP migration, (c) split-step Fourier shot-profile migration, and (d) 3D prestack Kirchhoff migration. Kirchhoff migration shows significant smiles below approximately 2 km of depth. Steep parts of the salt flanks are better imaged with Kirchhoff and common-azimuth by GSP migrations.

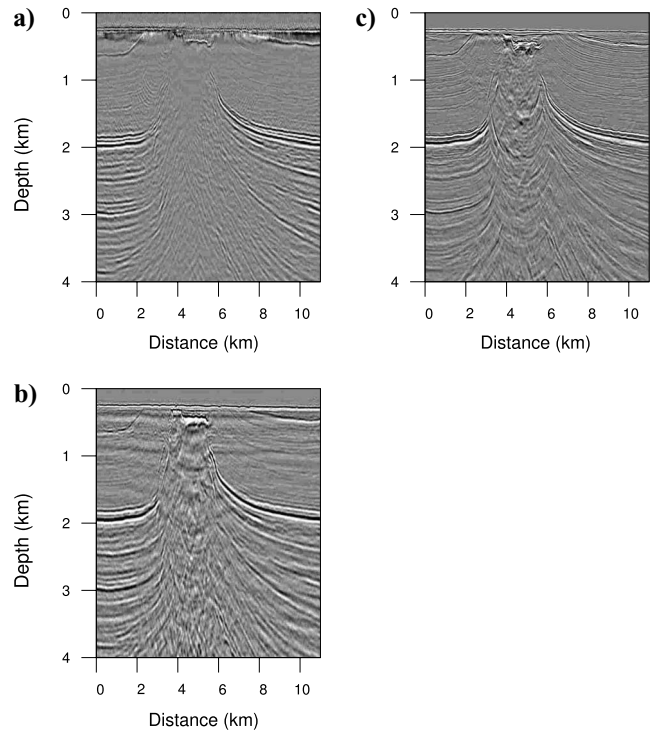Figure 10. Three–dimensional prestack migration for crossline 4500 using (a) shot-profile migration with explicit migration operators, (b) common-azimuth by GSP migration, and (c) Kirchhoff migration. Maximum frequency content in the migration with explicit migration operators and common-azimuth by GSP migration is 47 Hz and 45 Hz, respectively, although the maximum frequency used in the Kirchhoff migration is 55 Hz.

Raypaths in Figure 3 show multipathing does occur in areas close to the salt. Multipathing is difficult to manage for migration algorithms based on asymptotic ray theory (such as Kirchhoff migration using only a single arrival), and it might be of some significance for the appearance of artifacts in migrated depth sections (Hill, 2001; Geoltrain and Brac, 1993; Gray and May, 1994; and Le Rousseau et al., 2003).

The overall quality difference between migration using explicit migration operators and the split-step Fourier algorithm is not large: migration using explicit migration operators is only slightly better overall. However, close inspection of Figures 5 and Figures 8 reveals slight depth differences between split-step Fourier migration and migration using explicit operators. The split-step Fourier algorithm is correct only for velocity models with small lateral changes and waves with zero (or very small) wavenumbers. Arrivals with larger wavenumbers (or corresponding large dip angles) can be mispositioned. Because the final image is a stack over waves with both small and large wavenumbers, errors visible as phase changes or mispositioning (as in Figure 5) can occur. It is likely these errors would increase if a larger migration aperture were used because the larger aperture generally involves waves with larger wavenumbers.

The common-azimuth by GSP migration algorithm utilizes a migration operator based on the GSP method, which should be comparable in fidelity to explicit migration operators. Common-azimuth by GSP results in the previous section are similar to both shot-profile migration algorithms, but seem to be more noisy in areas close to the salt and deep in the section. However, common-azimuth migration involves additional assumptions for wave propagation in the crossline direction, which is not the case for the two shot-profile migration algorithms, and which is a possible source for less fidelity in the final image.

Computational cost for shot-profile migration with explicit operators relative to computational cost for split-step Fourier shot-profile migration is approximately a factor of four, as shown in Appendix A. Shot-profile migration cost using explicit operators relative to Kirchhoff migration depends to a large degree on the implementation of the Kirchhoff algorithm and the parameters used. It is approximately a factor of six for the salt data set used here, according to estimates in Appendix A. However, if maximum input frequency for Kirchhoff migration is reduced to the same maximum frequency used for shot-profile migration, the relative cost will increase to a factor of 25. In addition, if the Kirchhoff migration aperture is reduced to match the aperture for shot-profile migrations, the combined factor will reach approximately 40.

Appendix A also shows that common-azimuth by GSP migration for the salt data set is faster than shot-profile migration by a factor of approximately 90. If the same maximum frequency had been used for both migrations, the corresponding factor would be about 260.

The software used to perform shot-profile migrations is an in-house research implementation, although software for the common-azimuth GSP and Kirchhoff migration is commercial. Migrations were performed on a cluster with a variable number of CPUs. Accounting for this, observed relative run times for shot-profile and common-azimuth by GSP migrations agreed with cost estimates given above. Kirchhoff-migration run times were not measured accurately.

Clearly, shot-profile migration with explicit migration operators is less cost-effective than split-step Fourier shot-profile, Kirchhoff, or common-azimuth by GSP migration. Considering only the image quality in our data set, shot-profile migration using explicit migration operators yields slightly better images than shot-profile migration with the split-step Fourier approach, and clearly better results than common-azimuth by GSP and Kirchhoff migration.

The relatively high cost is the largest argument against the use of shot-profile migration with explicit operators. This could prevent using the method on large data sets. Still, for data sets of modest size (i.e., a few hundred square kilometers of marine streamer data), shot-profile migration using explicit migration operators should be a good alternative to other algorithms.

In addition, the above examples demonstrate that Kirchhoff migration using a single arrival only is not a good alternative in the area covered by the salt data set. The three wave-equation methods in our examples all show better image quality than Kirchhoff migration.

## CONCLUSION

Shot-profile migration based on explicit migration operators seems to be well suited for imaging in areas with complex geology and significant lateral velocity changes. Image quality in the explicit migration operator approach is slightly better than in split-step Fourier migration and clearly better than with common-azimuth by GSP and Kirchhoff migration in the studied data area.

Cost of using explicit migration operators is high, which makes the method less attractive in terms of efficiency than the comparable split-step Fourier approach or GSP algorithm. Kirchhoff migration that doesn't take multipathing into account does not seem to be well suited for imaging sediments in the part of the studied area with strong lateral velocity gradients.

Because our velocity model is constructed using Kirchhoff migration and ray-based tomography, questions can be raised on the accuracy and validity of the velocity model for producing the images shown in preceding sections. Even the best images appear not to be focused completely in the areas below salt structures. It is likely that a tomographic technique based on wave-equation approaches rather than on ray theory would lead to a better velocity model.

## ACKNOWLEDGMENTS

## APPENDIX A

### COMPUTATIONAL COST

Computational cost (measured in wall-clock computer time) of shot-profile migration with explicit operators and split-step Fourier shot-profile migration is dominated by the cost of wavefield extrapolation. Computation in both cases is performed on a regular grid with the number of nodes in the grid equal to $N_x^a N_y^a N_z$, where $N_x^a$ and $N_y^a$ are the number of grid points in the inline and crossline direction of the migration aperture at the surface, and $N_z$ is the number of grid nodes in depth. We assume computations are performed on a processor with limited internal memory, such that only one depth step of the velocity model and of the output image can be kept in memory. Cost

$r_e$ and $r_s$ of shot-profile migration with explicit operators and split-step shot-profile migration, respectively, can be written approximately as

$$r_e = 2AN_zN_fN_s(h\beta_e + 3g),$$

$$r_s = 2AN_zN_fN_s[h\beta_{fft}2\log_2(A) + 3g]. \quad (A\text{-}1)$$

Here $A = N_x^aN_y^a$ and the first factor of two on the right side come from the fact that both source and data must be extrapolated in depth. The inverse of the processor computation speed is denoted by $h$, measured in seconds per floating-point operations; $g$ is the inverse of the speed of transfer between memory and disk; and $\beta_e$ is the number of floating-point operations per grid node necessary to perform the migration. $N_f$ is the number of frequencies, and $N_s$ is the number of shots in the survey. Constant $\beta_{fft}$ is determined by the Fourier-transform algorithm.

The numerical value of $\beta_e$ is approximately $10^3$. Constants $h$ and $g$ are approximately $10^{-9}$ and $10^{-8}$ for present-day (2008) processors, respectively. It is immediately clear that the second term in the first equation of A-1 is insignificant and can be dropped, reflecting the fact that shot-profile migration with explicit migration operators is computationally bound (not depending on the speed of input-output operations to disk). Constant $\beta_{fft}$ is approximately equal to eight, so for reasonable values of $N_x^a = N_y^a \approx 10^3$, split-step Fourier migration is computationally bound also.

The cost given in equation A-1 can be expressed also in terms of the maximum frequency to be migrated by assuming that, optimally, sampling intervals of the computational grid are chosen as large as possible, but still fulfill the sampling theorem. Assuming $g = 0$ and horizontal sampling intervals are $\Delta x_e$ and $\Delta x_s$, then equation A-1 becomes

$$r_e = \left(\frac{2f_e^{\max}}{\Delta f}\right)A'\gamma_e^3L_zN_s(h\beta_e),$$

$$r_s = \left(\frac{2f_s^{\max}}{\Delta f}\right)A'\gamma_s^3L_zN_s[h\beta_{fft}2\log_2(A'\gamma_s^2)]. \quad (A\text{-}2)$$

Maximum migration frequencies are given by $f_e^{\max} = (2c_{\min}/\Delta x_e)$ and $f_s^{\max} = (2c_{\min}/\Delta x_s)$. Minimum velocity is $c_{\min}$, $\Delta f$ is the frequency sampling interval, $\gamma_e$ and $\gamma_s$ are defined by $\gamma_e = (2f_e^{\max}/c_{\min})$, and $\gamma_s = (2f_s^{\max}/c_{\min})$. The migration aperture is $A' = L'_xL'_y$, where $L'_x$ and $L'_y$ are the lengths and widths of the migration aperture and $L_z$ is the maximum depth, all measured in meters.

The computational cost for common-azimuth by GSP migration (Biondi, 2006) is denoted by $r_c$ and is approximately equal to

$$r_c = N_zN_fB[h\beta_{fft}(s + 2)N_h\log_2(N_xN_yN_h) + 3g], \quad (A\text{-}3)$$

where $B = N_xN_y$, and $N_x$ and $N_y$ are the number of grid points in the inline and crossline directions of the entire survey area. The order of the GSP algorithm is equal to $s$, and $N_h$ is the number of traces in a CMP gather. We have assumed that the entire input data set for one frequency can be kept in memory, although only one depth step of the velocity model and output image is kept in memory. The second term in equation A-3 is much smaller than the first term, so it can be neglected in practice in the same way as for shot-profile migration.

Equation A-3 can be expressed as the function of the maximum frequency. For $g = 0$, we get

$$r_c = L_z\left(\frac{f_c^{\max}}{\Delta f}\right)\gamma_c^3B'N_h[h\beta_{fft}(s + 2)\log_2(B'\gamma_c^2N_h)], \quad (A\text{-}4)$$

where $B' = L_xL_y$ and $L_x, L_y$, and $L_z$ are the length, width, and depth of the image volume measured in meters, respectively. $f_c^{\max}$ and $\gamma_c$ are defined in a similar way as corresponding quantities for the shot-profile migrations.

The computational cost of Kirchhoff migration (Biondi, 2006) is given as

$$r_k = AN_hBN_z(h\beta_k + 2g), \quad (A\text{-}5)$$

where we have assumed the output image is not kept in memory. A reasonable value of $\beta_k$ is in the range of 5–30 (Biondi, 2006), so for present-day computers, the second term cannot be neglected. This reflects the fact that Kirchhoff migration is not computationally bound, but relies just as much on the speed of input-output operations to disk as on the computational speed of processors. We will use the approximation that input-output operations are equally as expensive as the computational operations, $2g \approx h\beta_k$.

In addition, the above equation for the cost of Kirchhoff migration can be expressed in principle as a function of frequency. Assuming the input data grid is fixed for all frequencies, with sampling interval in the horizontal directions equal to $\Delta x_d$ and $\Delta y_d$, and using the same spatial sampling intervals in the image space as for the wave-equation migrations discussed above, we get

$$r_k = \left(\frac{A'_k}{\Delta x_d\Delta y_d}\right)N_h\gamma_k^3B'L_z2h\beta_k. \quad (A\text{-}6)$$

Here, $A'_k$ is the area of the Kirchhoff migration aperture.

Using equations A-2, A-4, and A-6, we obtain the ratios between computational cost of shot-profile migration with explicit operators and split-step Fourier shot-profile migration, common-azimuth by GSP migration, and Kirchhoff migration as

$$r_e/r_s = \left(\frac{f_e}{f_s}\right)^4\frac{\beta_e}{\beta_{fft}2\log_2(A'\gamma_s^2)},$$

$$r_e/r_c = \left(\frac{f_e}{f_c}\right)^4\left(\frac{2A'N_s}{B'N_h}\right)\frac{\beta_e}{\beta_{fft}(s + 2)\log_2(B'N_h\gamma_c^2)},$$

$$r_e/r_k = \left(\frac{f_e}{\Delta f}\right)\left(\frac{f_e}{f_k}\right)^3\left(\frac{A'\Delta x_d\Delta y_dN_s}{A'_kB'N_h}\right)\left(\frac{\beta_e}{\beta_k}\right). \quad (A\text{-}7)$$

The above expressions must be taken with some caution because details of implementation and computer hardware might influence the results to a considerable degree.

For the salt data set described here, output image dimensions are equal to $L_x = 16$ km, $L_y = 11$ km, and $L_z = 4$ km. This gives $r_e/r_s \approx 4$. The nominal fold of the survey is 30, and the number of shots $N_s = 80,000$, and the shot-profile migration aperture is $L'_x = L'_y = 6$ Km. Common-azimuth by GSP migration had a maximum frequency of 45 Hz and the number of offsets was increased to 150 because of the sampling requirement in the offset domain. With $s = 2$, this gives $r_e/r_{ca} \approx 90$. Reducing maximum frequency of the common-azimuth by GSP migration to the same maximum frequency

used in shot-profile migrations (35 Hz) gives $r_e/r_c \approx 260$. Reducing the order of the GSP migration operator to zero gives $r_e/r_c \approx 530$.

The maximum frequency used in Kirchhoff migration is approximately 55 Hz, sampling intervals were $\Delta x_d = 12.5$ m and $\Delta y_d = 25.0$ m, and the radius of the circular migration aperture was 4.5 km, which gives $r_e/r_k \approx 6$. Here we have used $\beta_k = 15$. Reducing the maximum frequency of the Kirchhoff migration to the same as for shot-profile migrations gives $r_e/r_k \approx 25$. In addition, reducing migration aperture to that of the shot-profile migrations gives $r_e/r_k \approx 40$.

# REFERENCES

Albertin, U., C. Stork, D. Yingst, W. Chang, R. Fletcher, and P. Kitchenside, 2004, Amplitude behaviour of Kirchhoff, wavefield extrapolation, and beam migration in areas of poor illumination: 66th Annual Conference and Technical Exhibition, EAGE, Extended Abstracts, G25.

Biondi, B., 2006, 3D seismic imaging: Society of Exploration Geophysicists.

Biondi, B., and G. Palacharla, 1996, 3D prestack migration of common-azimuth data: Geophysics, **61**, 1822–1832.

Blacquière, G., H. Debeye, C. Wapenaar, and A. Berkhout, 1989, 3D table-driven migration: Geophysical Prospecting, **37**, 925–958.

Claerbout, J. F., 1971, Toward a unified theory of reflector mapping: Geophysics, **36**, 467–481.

De Hoop, M. V., J. H. Le Rousseau, and R. S. Wu, 2000, Generalization of the phase-screen approximation for the scattering of acoustic waves: Wave Motion, **31**, 52–74.

Geoltrain, S., and J. Brac, 1993, Can we image complex structures with first-arrival traveltime?: Geophysics, **58**, 564–575.

Gray, S. H., and W. P. May, 1994, Kirchhoff migration using eikonal traveltimes: Geophysics, **59**, 810–817.

Hale, D., 1991a, 3D depth migration via McClellan transformations: Geophysics, **56**, 1778–1785.

——, 1991b, Stable explicit depth extrapolation of seismic wavefields: Geophysics, **56**, 1770–1777.

Hill, N. R., 2001, Prestack gaussian-beam depth migration: Geophysics, **66**, 1240–1250.

Holberg, O., 1988, Towards optimum one-way wave propagation: Geophysical Prospecting, **36**, 99–114.

Le Rousseau, J. H., H. Calandra, and M. V. De Hoop, 2003, Three-dimensional depth imaging with generalized screens: A salt body case study: Geophysics, **68**, 1132–1139.

Le Rousseau, J. H., and M. V. De Hoop, 2001, Modeling and imaging with the scalar generalized-screen algorithms in isotropic media: Geophysics, **66**, 1551–1568.

Mittet, R., 2007, Explicit 3D depth migration with a constrained operator: Geophysics, **71**, S63–S71.

Sollid, A., and B. Arntsen, 1994, Cost effective one-pass 3D depth migration: Geophysical Prospecting, **42**, 755–776.

Soubaras, R., 1992, Explicit 3D migration using equiripple polynomial expansion and Laplacian synthesis: 62nd Annual International Meeting, SEG, Expanded Abstracts, 905–908.

Stoffa, P. L., J. T. Fokkema, R. M. L. Freire, and W. P. Kessinger, 1990, split-step Fourier migration: Geophysics, **55**, 410–421.

Vinje, V., E. Iversen, and H. Gjøystdal, 1993, Traveltime and amplitude estimation using wavefront construction: Geophysics, **58**, 1157–1166.